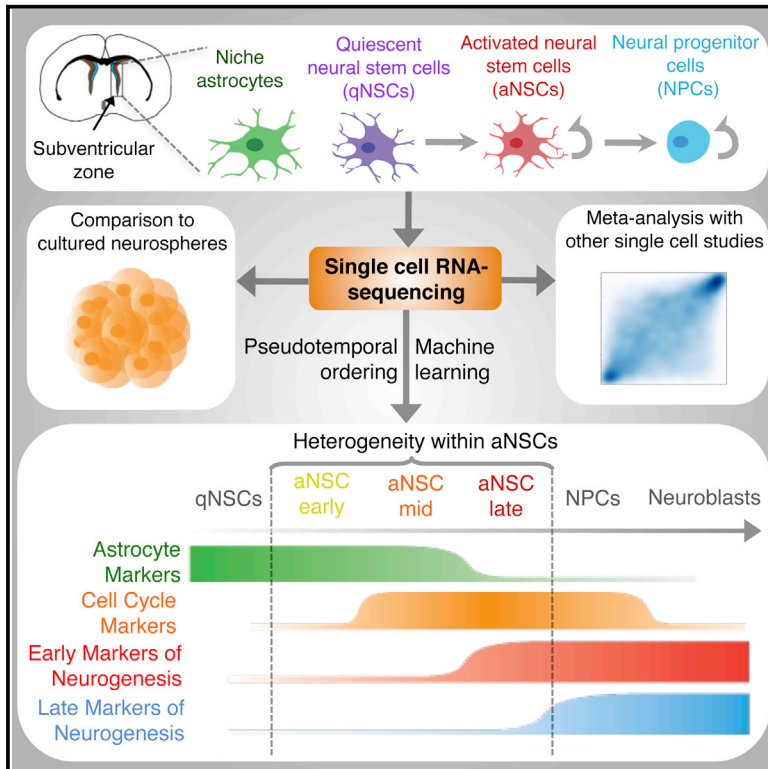# Single-Cell Transcriptomic Analysis Defines Heterogeneity and Transcriptional Dynamics in the Adult Neural Stem Cell Lineage

Graphical Abstract

Authors

Ben W. Dulken, Dena S. Leeman, Stéphane C. Boutet, Katja Hebestreit, Anne Brunet

Correspondence

abrunet1@stanford.edu

In Brief

Dulken et al. perform single-cell transcriptomics on neural stem cells (NSCs) from adult mice. They use machine learning to identify rare intermediate cells in the continuum of the NSC lineage and perform a meta-analysis with other single-cell transcriptomic data from in vitro or in vivo NSCs.

Highlights

- Single-cell RNA-seq to characterize adult neural stem cell populations

- Machine learning and pseudotemporal ordering show a continuum in the lineage

- Validation of an intermediate state in the neural stem cell population

- Meta-analysis with other in vitro and in vivo single-cell datasets

CrossMark

CellPress

Single-Cell Transcriptomic Analysis Defines Heterogeneity and Transcriptional Dynamics in the Adult Neural Stem Cell Lineage

Ben W. Dulken,[1,2,3] Dena S. Leeman,[1,4] Stéphane C. Boutet,[5] Katja Hebestreit,[1] and Anne Brunet[1,6,7,*]
[1]Department of Genetics, Stanford University, Stanford, CA 94305, USA
[2]Stanford Medical Scientist Training Program, Stanford University, Stanford, CA 94305, USA
[3]Institute for Stem Cell Biology and Regenerative Medicine, Stanford University, Stanford, CA 94305, USA
[4]Cancer Biology Program, Stanford University, Stanford, CA 94305, USA
[5]Fluidigm Corporation, South San Francisco, CA 94080, USA
[6]Glenn Laboratories for the Biology of Aging at Stanford University, Stanford University, Stanford, CA 94305, USA
[7]Lead Contact
*Correspondence: abrunet1@stanford.edu
http://dx.doi.org/10.1016/j.celrep.2016.12.060

SUMMARY

Neural stem cells (NSCs) in the adult mammalian brain serve as a reservoir for the generation of new neurons, oligodendrocytes, and astrocytes. Here, we use single-cell RNA sequencing to characterize adult NSC populations and examine the molecular identities and heterogeneity of in vivo NSC populations. We find that cells in the NSC lineage exist on a continuum through the processes of activation and differentiation. Interestingly, rare intermediate states with distinct molecular profiles can be identified and experimentally validated, and our analysis identifies putative surface markers and key intracellular regulators for these subpopulations of NSCs. Finally, using the power of single-cell profiling, we conduct a meta-analysis to compare in vivo NSCs and in vitro cultures, distinct fluorescence-activated cell sorting strategies, and different neurogenic niches. These data provide a resource for the field and contribute to an integrative understanding of the adult NSC lineage.

INTRODUCTION

Populations of neural stem cells (NSCs) in the adult brain represent a critical reservoir of regenerative cells with the potential to combat neuronal injury and neurodegeneration. The adult brain contains two NSC pools located in the sub-ventricular zone (SVZ) of the lateral ventricles and the dentate gyrus (DG) of the hippocampus (Zhao et al., 2008). Both NSC pools produce new neurons that can integrate into functional circuits (Zhao et al., 2008). The NSCs of the SVZ have been identified as a subtype of sub-ependymal astrocytes (Doetsch et al., 1999; Garcia et al., 2004). The majority of NSCs are quiescent and express glial fibrillary acidic protein (GFAP) along with the marker CD133 (Prominin 1) (Codega et al., 2014; Fischer et al., 2011). These quiescent NSCs (qNSCs or type B1q cells) give rise to proliferative, activated neural stem cells

(aNSCs or type B1a cells) that express epidermal growth factor receptor (EGFR) (Codega et al., 2014). Activated NSCs can, in turn, produce neural progenitor cells (NPCs or transient amplifying progenitors [TAPs] or type C cells), a proliferative cell population that expresses markers of early neuronal differentiation (Doetsch et al., 2002). Finally, the NPCs give rise to neuroblasts (type A cells) that migrate to the olfactory bulb, where they become primarily interneurons (Garcia et al., 2004; Mirzadeh et al., 2008; Figure 1A).

The purification of NSCs from their in vivo niche has been made possible by fluorescence-activated cell sorting (FACS) via the expression of transgenic markers and defined surface markers (Codega et al., 2014; Fischer et al., 2011; Garcia et al., 2004; Mich et al., 2014). Purification of cell populations, coupled to gene expression profiling, has begun to reveal the molecular identities of NSCs in the SVZ (Codega et al., 2014; Mich et al., 2014). However, population-based approaches have likely obscured the underlying heterogeneity in the NSC lineage, thereby limiting the identification of new rare cell types or intermediates and hindering the characterization of complex transcriptional dynamics. Although recent single-cell studies have started to reveal the complex composition of NSC populations in various neurogenic regions of the adult brain, the SVZ (Llorens-Bobadilla et al., 2015; Luo et al., 2015), and the DG (Shin et al., 2015), a comprehensive molecular understanding of the heterogeneity of the neural stem cell lineage remains elusive.

Here we perform single-cell RNA sequencing on 329 high-quality single cells from four different populations—niche astrocytes, qNSCs, aNSCs, and NPCs—freshly isolated from young adult mouse SVZs. Using machine learning and pseudotemporal ordering, we reveal subpopulations of NSCs along the spectrum of activation and differentiation, which we experimentally validate, and suggest putative markers for these subpopulations. Using the power of single-cell transcriptomics, we compare our single-cell dataset to other single-cell datasets, including in vitro-cultured NSCs and other in vivo NSC datasets. Our findings not only serve as a great resource for the field but also provide an integrative understanding of the neural stem cell lineage, which is an essential step toward identifying new ways to reactivate dormant NSCs in the context of stroke and aging.
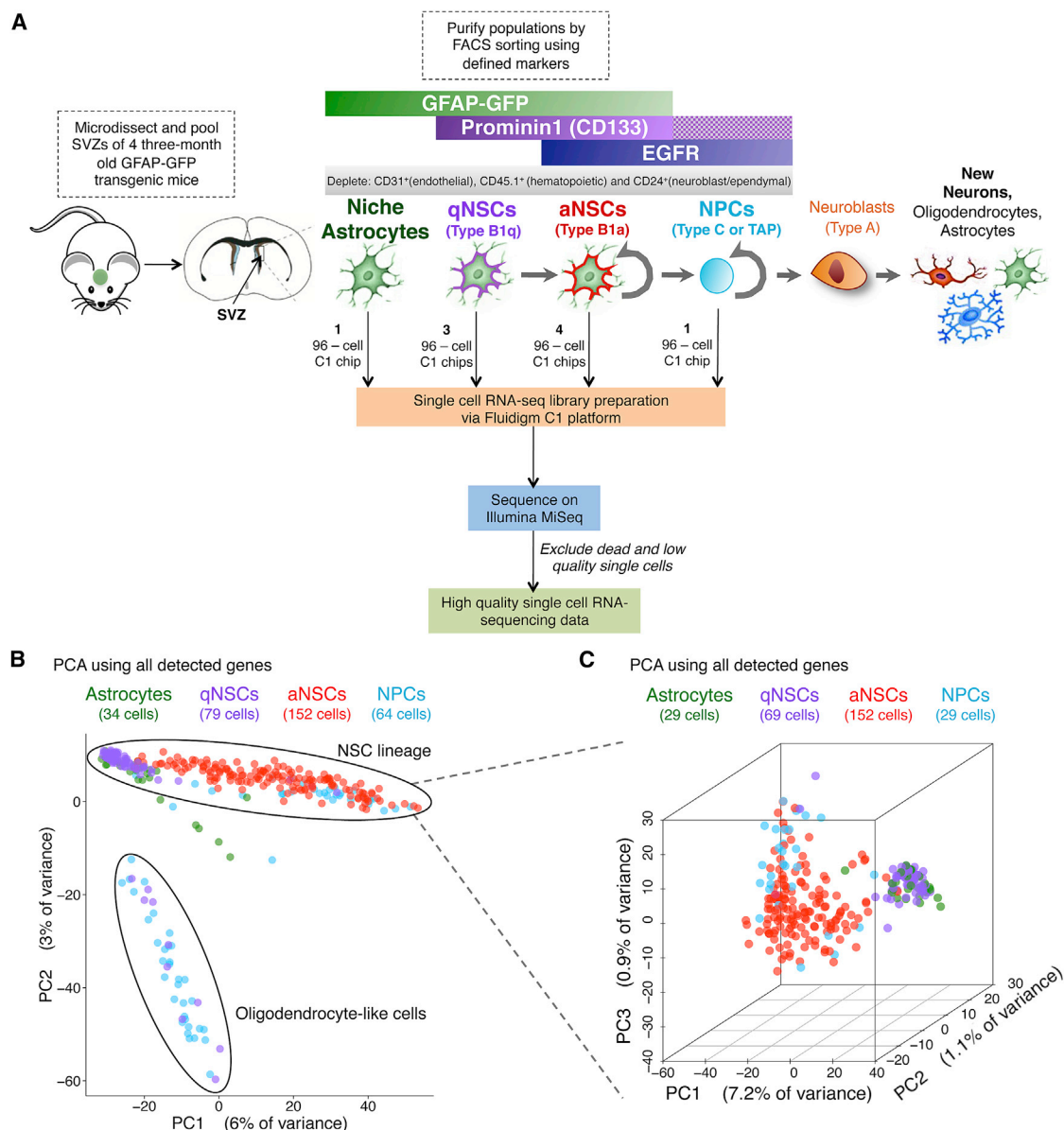
Figure 1. Single-Cell RNA-Seq of 329 Cells from Four Populations of FACS-Purified Cells from the SVZs of Adult Mice
(A) FACS scheme for the enrichment of astrocytes, qNSCs, aNSCs, and NPCs from the SVZs of adult mice and microfluidic-based single cell RNA-seq library generation and sequencing. The checkered bar in the FACS scheme indicates that the presence of Prominin 1 was not selected for. Note that, although Prominin 1 enriches for NSCs, the astrocyte population could contain some qNSCs, and the qNSC population could contain some astrocytes (Codega et al., 2014).
(B) Principal component analysis (PCA) of all 329 high-quality single cells.
(C) Three-dimensional PCA of all 288 cells, excluding oligodendrocyte-like cells and seven outlying cells.

RESULTS

Single-Cell RNA-Seq from Four Populations of Cells Directly Isolated from the SVZ Regenerative Region in the Adult Mouse Brain

To define the molecular heterogeneity of the SVZ regenerative region in the adult mouse brain, we performed single-cell RNA-sequencing from four cell populations—niche astro-

cytes, quiescent and activated NSCs, and more committed NPCs. We implemented a well-accepted FACS protocol to freshly isolate adult populations from the SVZ (Codega et al., 2014) using a transgenic line in which GFP is under the control of the human *GFAP* promoter (GFAP-GFP mice) (Zhuo et al., 1997). Single cells were dissociated from microdissected SVZs from young adult (3 months old) GFAP-GFP male mice and stained with markers of NSC identity and

activation, including CD133/Prominin 1 (PROM1) and EGFR. This approach enabled us to isolate niche astrocytes (henceforth referred to as astrocytes) (GFAP-GFP$^+$PROM1$^-$EGFR$^-$), qNSCs (GFAP-GFP$^+$PROM1$^+$EGFR$^-$), aNSCs (GFAP-GFP$^+$PROM1$^+$EGFR$^+$), and NPCs (GFAP-GFP$^-$EGFR$^+$), as described in Codega et al. (2014) (Figure 1A; Figure S1A). Each of these enriched populations was used to prepare single-cell RNA-sequencing libraries using the Fluidigm C1 Single-Cell Auto Prep microfluidic system (Wu et al., 2014). A total of 524 single cell libraries were sequenced on Illumina MiSeq, and a subset was also sequenced on Illumina HiSeq 2000 (Tables S1, S2, S3, and S4). The majority of unique genes in each library were detected by MiSeq (Figure S1B), and there was good correlation between gene detection for libraries sequenced on MiSeq and HiSeq for all genes except those expressed at very low levels (Figure S1C), consistent with previous observations that high sequencing depth is not necessary to capture single-cell library complexity (Pollen et al., 2014). We excluded low-quality cells based on a threshold for reads mapping to the transcriptome and number of genes detected (Figure S1D). On the remaining 329 cells, there was good correlation of gene expression between two representative single cells (Pearson correlation = 0.602) or pseudopopulations (Pearson correlation = 0.932) (Figure S1E). Furthermore, aggregated single-cell pseudopopulations for each cell type cluster with population RNA sequencing (RNA-seq) (D.S.L., K.H., and A.B., unpublished data) for their associated cell type and away from a cell type from an independent lineage (endothelial cells) (Figures S1F and S1G), underscoring the quality of the single-cell RNA-seq libraries.

To explore the molecular identities of individual single cells, we performed global principal component analysis (PCA) projection of all single cells profiled in this analysis. Most astrocytes, qNSCs, aNSCs, and NPCs clustered in a well-defined "band," although a subpopulation of cells sorted as qNSCs and NPCs separated significantly from the majority of the single cells on the second principal component (PC) of the PCA (Figure 1B). Genes with the strongest contribution to this second PC were highly enriched for genes involved in myelination and oligodendrocyte function/identity (e.g., *Mog*, *Plp1*, and *Mbp*) (Cahoy et al., 2008; Figure S1H). Thus, a minority of oligodendrocytes appear to be present in the population of cells sorted as qNSCs and NPCs, which was also observed in another single-cell study (Llorens-Bobadilla et al., 2015).

To focus our analysis on the NSC lineage, we excluded all cells exhibiting an oligodendrocyte expression signature as well as a small number of outlying cells that clustered away from the NSC lineage (Figure 1B). PCA on the remaining cells revealed clustering of the more quiescent cell types (astrocytes and qNSCs) away from the active, proliferative cell types (aNSCs and NPCs) (Figure 1C). Although there was no significant difference between astrocytes and qNSCs, consistent with previous studies (Codega et al., 2014), aNSCs separated from NPCs (Figure 1C). Interestingly, a range of aNSCs was observed between the quiescent and progenitor states (Figure 1C), raising the possibility that in vivo NSCs exist on a continuum of quiescence, activation, and differentiation.

Single Cells from Populations of qNSCs, aNSCs, and NPCs Can Be Ordered through Activation and Differentiation, Suggesting Heterogeneity and Intermediary States

To explore the intermediary states in the continuum of NSCs and progeny, we performed pseudotemporal ordering of the single cells using Monocle (Trapnell et al., 2014). Because astrocytes and qNSCs could not be distinguished by PCA (Figure S2A) or differential expression (Table S5), we omitted astrocytes from the Monocle ordering analysis. Monocle ordering on qNSCs, aNSCs, and NPCs using all detected genes revealed gene expression dynamics that recapitulate the previous understanding of the activation of NSCs (Figures 2A and 2B). Indeed, qNSCs that highly express previously reported markers of this population, such as *Id3* (Bonaguidi et al., 2008; Mira et al., 2010), are ordered first and are followed by aNSCs that have upregulated *Egfr* (Figure 2B). As cells transition from qNSCs to aNSCs, they first upregulate genes important for ribosomal biogenesis (e.g., *Rpl32*) before expressing markers of the cell cycle (Figure 2B). This corroborates a recent study that described an early stage of biogenesis in aNSCs prior to cell cycle entry (Llorens-Bobadilla et al., 2015). To experimentally validate the existence of this population of "cell cycle-low" aNSCs, we stained populations of qNSCs, aNSCs, and NPCs sorted by FACS with the cell cycle marker Ki67. Consistent with our single cell prediction, a fraction of aNSCs was negative for the Ki67 cell cycle marker (Figure 2C), and the proportion of Ki67-negative cells was significantly greater in the aNSC population than in NPCs (Figure 2D). These results indicate that a subpopulation of aNSCs is not cycling but that these cell cycle-low aNSCs are, in fact, already expressing the EGFR *protein*, based on the FACS approach we used, rather than merely expressing the *Egfr transcript* and preparing to enter an EGFR-positive state.

Monocle ordering could not place NPCs after aNSCs, perhaps because genes highly expressed in both cell types (e.g., cell cycle, metabolism genes) masks more subtle transcriptomic changes. Therefore, to increase the sensitivity of Monocle ordering to the process of lineage commitment/differentiation, we built machine learning models to identify the genes most important for defining the trajectory of cells through four states (Figure 2E): qNSCs, cell cycle-low aNSC, "cell cycle-high" aNSC, and NPCs. We implemented a four-way stochastic gradient-boosting classification model (Friedman, 2002) using a subsampled set of 20 cells from each of these four groups ("training set") (Figure 2E; code available at https://github.com/bdulken/SVZ_NSC_Dulken_2). We bootstrapped this process by building 100 independent models using independently sampled subsets of single cells (Figure 2E). In predicting the identity of cells that were not used to build the model ("testing set"), the accuracy of the models was approximately 80% (Figure S2B), indicating that the models perform drastically better than random assignment in predicting cell state. Machine learning also identifies the genes that are most important for the construction of the models (Table S6). Of these, we selected the genes found in the top 100 most important features in at least half of the models, producing a list of 34 genes, several of which were previously known to be dynamically regulated during NSC activation and differentiation (e.g., *Clu*, *Ccnd2*, *Dlx2*, and *Dcx*)
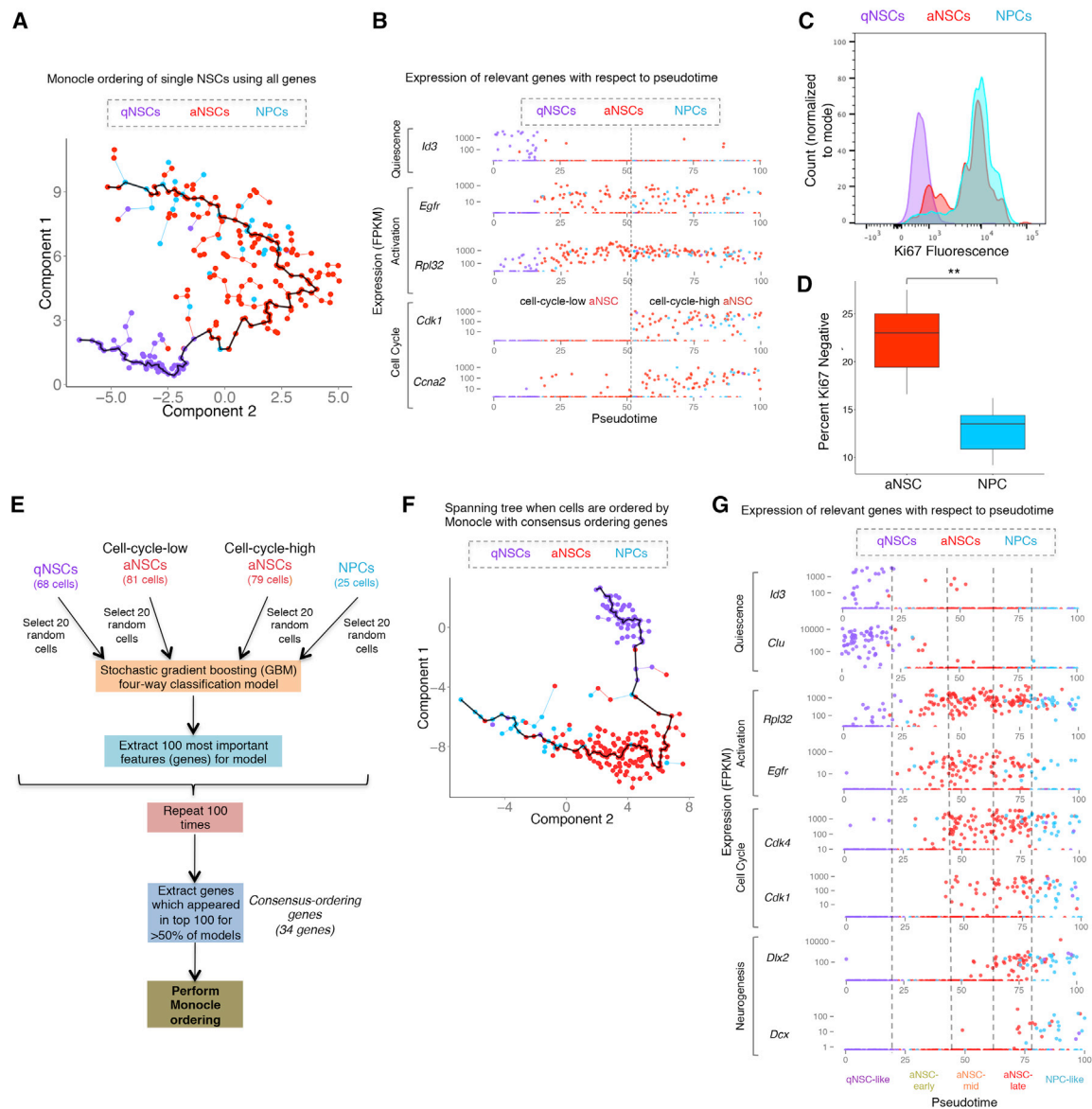
Figure 2. Ordering of Single Cells from Populations of qNSCs, aNSCs, and NPCs Reveals Transcriptional Dynamics and Suggests Intermediary States

(A) Minimum spanning tree generated for all qNSCs, aNSCs, and NPCs ordered by Monocle using all detected genes.

(B) Expression of key genes associated with quiescence (*Id3*), activation (*Egfr* and *Rpl32*), and the cell cycle (*Cdk1* and *Ccna2*) (fragments per kilobase of transcript per million reads [FPKM]) in each cell, plotted with respect to pseudotime produced by Monocle in Figure 2A. Cells are color-coded by their FACS identity.

(C) Histogram of Ki67 fluorescence values measured by intracellular FACS in purified populations of qNSCs, aNSCs, and NPCs. Histogram values were normalized to mode.

(D) Percentage of Ki67-negative cells measured by intracellular FACS in purified populations of aNSCs and NPCs (two-sided Wilcoxon signed-rank test, **p ≤ 0.005).

(E) Machine learning algorithm to obtain consensus-ordering genes. The list of consensus-ordering genes is shown in Table S7.

(F) Minimum spanning tree generated for all qNSCs, aNSCs, and NPCs ordered by Monocle using FPKM of the consensus-ordering genes (Table S7).

(G) Expression (FPKM) of key genes related to quiescence (*Id3*), activation (*Egfr* and *Rpl32*), the cell cycle (*Cdk4* and *Cdk1*), and neuronal differentiation (*Dlx2* and *Dcx*) (FPKM) in each cell is plotted with respect to pseudotime produced by Monocle when all qNSCs, aNSCs, and NPCs are ordered using the consensus-ordering genes. Cells are color-coded by their FACS identity (indicated at the top). Bottom: name of the intermediary states (qNSC-like, aNSC-early, aNSC-mid, aNSC-late, and NPC-like).
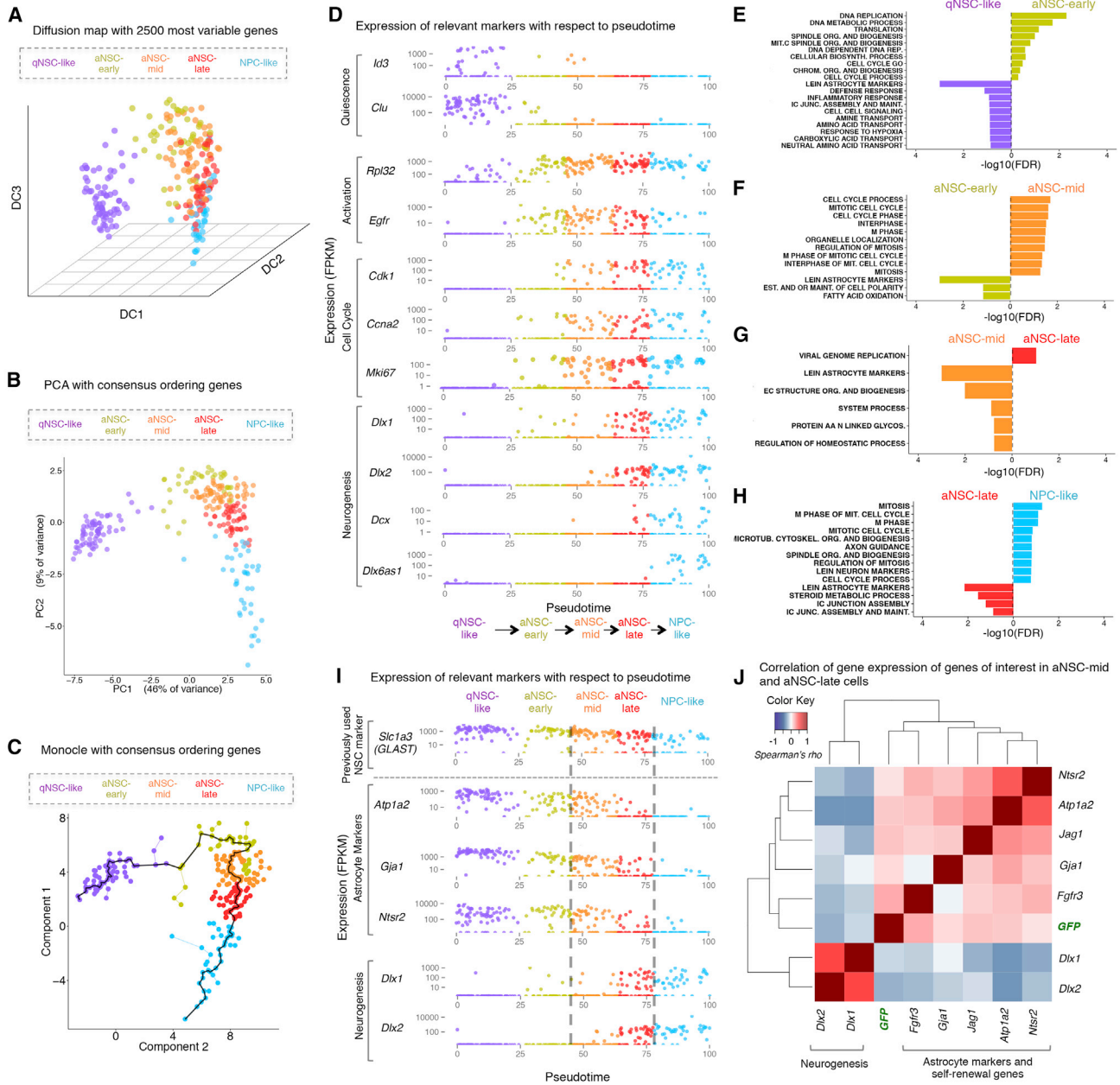
Figure 3. Activated NSCs Can Be Divided into Specific Subpopulations, Defined by the Expression of Specific Genes, along the Spectrum of Activation and Differentiation

(A) Diffusion map using the 2,500 most variable genes in the dataset for all qNSCs, aNSCs, and NPCs. Cells are colored by the identity of the intermediate states defined in Figure 2G.

(B) PCA using the consensus-ordering genes (Table S7) for all qNSCs, aNSCs, and NPCs. Cells are colored as in (A).

(C) Spanning tree produced by Monocle when all qNSCs, aNSCs, and NPCs are ordered using the consensus-ordering genes (Table S7). The black line represents the pseudotime "track" through the single-cell lineage. Cells are colored as in (A).

(D) Expression (FPKM) of genes relevant to the transition between the indicated stages in each cell, plotted with respect to pseudotime produced by Monocle when all qNSCs, aNSCs, and NPCs are ordered using the consensus-ordering genes (Table S7). Cells are colored as in (A).

(E–H) Gene set enrichments for genes ranked by Z score for differential expression between cells in intermediate states defined in (A). Enrichments are expressed as ($-$log10 [false discovery rate, FDR]), and directionality and color indicate the intermediate state in which the gene set is enriched. Comparisons shown for (E) qNSC-like versus aNSC-early, (F) aNSC-early versus aNSC-mid, (G) aNSC-mid versus aNSC-late, and (H) aNSC-late versus NPC. The gene sets presented are those for which FDR < 0.2.

(legend continued on next page)

(Table S7). When Monocle-based cell ordering was conducted using this subset of 34 "consensus-ordering" genes, it resulted in a strikingly accurate recapitulation of the current understanding of activation and commitment/differentiation of NSCs and their progeny (Figure 2G; Figure S2C; Codega et al., 2014; Doetsch et al., 2002; Llorens-Bobadilla et al., 2015). Monocle ordering with the consensus-ordering genes not only orders qNSCs first, followed by aNSCs negative for cell cycle markers, but also captures the dynamics of differentiation (Figure 2G). Indeed, a subset of aNSCs expressing cell cycle markers also exhibits expression of *Dlx2*, a pro-neural transcription factor known to promote neural differentiation (Doetsch et al., 2002; Petryniak et al., 2007; Suh et al., 2009). These cells are ordered later in pseudotime than other aNSCs, closely juxtaposed with NPCs (Figure 2G). Thus, a subpopulation of aNSCs may exhibit an early transcriptomic signature of neural differentiation. NPCs themselves are predominantly ordered last and express other important regulators and indicators of neurogenesis, such as *Dcx*, *Sp8*, and *Sp9* (Figure 2G; Figure S2C; Hsieh, 2012; Long et al., 2009; Waclaw et al., 2006). Other important regulators of neurogenesis, such as *Ascl1* and *Pax6*, are expressed throughout the aNSC and NPC populations (Figure S2C), consistent with evidence that *Ascl1* is both required for quiescent cells to enter the active state and for neuronal differentiation (Andersen et al., 2014). Together, the dynamic expression of key markers along this continuum of activation and differentiation suggests five distinct consecutive molecular states: qNSC-like ($Egfr^-$), aNSC-early ($Egfr^+Cdk1^-$), aNSC-mid ($Egfr^+Cdk1^+Dlx2^{low}$), aNSC-late ($Egfr^+Cdk1^+Dlx2^{high}$), and NPC-like ($Dlx2^+Dcx^+$) (Figure 2G; Figures S2C and S3B; Table S8).

Thus, machine learning identifies specific consensus-ordering genes that can order NSCs and progeny and suggests the existence of new intermediate states of activation and differentiation within the aNSC population.

Activated NSCs Can Be Divided into Specific Subpopulations, Defined by the Expression of Markers, along the Spectrum of Activation and Differentiation

To independently corroborate the subpopulations identified by machine learning and Monocle ordering (qNSCs-like, aNSC-early, aNSC-mid, aNSC late, and NPC-like), we used diffusion mapping, which has been recently developed to plot cells with respect to their molecular trajectories (Haghverdi et al., 2015). Diffusion mapping with the 2,500 most variable genes (Figure 3A) or all detected genes (Figure S3A) clusters the cells in a similar manner as Monocle or PCA using the consensus-ordering genes (Figures 3B–3D), confirming our machine learning approach.

To define the gene expression changes occurring between all five states (qNSC-like, aNSC-early, aNSC-mid, aNSC-late, and NPC-like), we conducted differential expression analysis at each cell state transition using the single-cell differential expression tool single cell differential expression (SCDE) (Kharchenko

et al., 2014) and assessed pathway enrichment using gene set enrichment analysis (GSEA) (Table S8). The transition from qNSC-like to aNSC-early is characterized by upregulation of genes belonging to ribosomal signatures (Figures 3D and 3E), confirming our earlier observations (Figure 2) and findings from another single-cell study in the SVZ (Llorens-Bobadilla et al., 2015). As expected, the transition from aNSC-early to aNSC-mid is characterized by upregulation of genes belonging to cell cycle signatures (Figures 3D and 3F). The transition between the aNSC-mid and aNSC-late cell states is defined partly by the upregulation of *Dlx1* and *Dlx2*, two genes normally associated with neuronal differentiation (Petryniak et al., 2007; Figure 3D). However, aNSC-late cells did not express the other genes that are characteristic of the NPC-like population, such as *Dcx*, *Nrxn3*, *Dlx6as1*, *Sp8*, and *Sp9* (Figure 3D; Figure S3C), suggesting that aNSC-late are distinct from NPCs. Interestingly, the transition from aNSC-mid to aNSC-late is characterized by downregulation of genes relating to astrocyte identity (Figure 3G), such as *Atp1a2*, *Gja1*, and *Ntsr2* (Cahoy et al., 2008; Figure 3I). Astrocytic markers are further downregulated as cells transition into the NPC-like state (Figures 3H and 3I). Thus, aNSCs that highly express cell cycle genes can be further sub-divided into two groups, a group still expressing astrocyte markers (characteristic of earlier cells in the lineage) and a group in which early neurogenesis markers begin to be expressed. These two states could represent the division between a self-renewing NSC and a lineage-committed NSC primed for differentiation.

This analysis also enables us to identify putative markers or regulators that may be specific to these earlier, potentially self-renewing NSCs. Indeed, although *GLAST* (*Slc1a3*) has been previously used as a marker to detect NSCs (Llorens-Bobadilla et al., 2015; Mich et al., 2014), it is actually expressed in aNSC-mid, aNSC-late, and NPCs (Figure 3I). In contrast, other markers appear to be more specific to the aNSC-mid subtype, including the cell surface genes *Atp1a2*, *Gja1*, and *Ntsr2* (Figure 3I). Although these genes are also expressed in other cell types in the brain, including cortical astrocytes, they could serve to isolate the aNSC-mid group in combination with other markers of NSCs. Furthermore, *Jagged1* and *Fgfr3*, which have been implicated in NSC self-renewal (Maric et al., 2007; Nyfeler et al., 2005), are among the genes elevated in the aNSC-mid cells (Figure S3D) and could also potentially serve as markers in combination with other NSC markers. Interestingly, genes that are enriched in the aNSC-mid population, including markers of astrocytes (*Atp1a2*, *Ntsr2*, and *Gja1*) and mediators of self-renewal (*Fgfr3* and *Jag1*), are correlated with each other and anti-correlated with genes associated with the aNSC-late population, *Dlx1* and *Dlx2*, in the aNSC-mid and aNSC-late states (Figure 3J; Figure S3F). Collectively, these data support the notion that the division between the aNSC-mid and aNSC-late populations is associated with the loss of astrocytic gene signatures and the acquisition of a pro-neural gene expression signature.

(I) Expression (FPKM) of markers of astrocytes (*Atp1a2*, *Gja1*, and *Ntsr2*) and neurogenesis (*Dlx1* and *Dlx2*) in each cell plotted as a function of pseudotime. *GLAST* (*Slc1a3*), a marker of astrocytes that was previously used in FACS studies, is presented as a comparison at the top. Cells are colored as in (A).

(J) Markers of astrocytes (*Atp1a2*, *Ntsr2*, and *Gja1*) and mediators of self-renewal (*Jag1* and *Fgfr3*) are correlated with each other and are anticorrelated with early markers of neuronal differentiation (*Dlx1* and *Dlx2*) in aNSC-mid and aNSC-late cells. The carpet plot shows correlation (Spearman's rho) between individual genes in all aNSC-mid and aNSC-late cells.

Experimental Validation of Single-Cell Data Prediction by Purifying aNSC Subpopulations Using the Level of GFAP-GFP Expression

We next experimentally validated the existence of specific aNSC subpopulations. The *GFAP-GFP* transgene is known to be downregulated as NSCs commit to the NPC state (Doetsch et al., 2002; Pastrana et al., 2009; Figure 4A). Indeed, *GFP* transcript levels from the *GFAP-GFP* transgene positively correlate with markers of astrocytes and negatively correlate with early markers of neurogenesis in aNSCs (Figure 3J). We therefore used FACS to sort different populations of aNSCs based on their level of GFP fluorescence from the *GFAP-GFP* transgene. Because we did not know the levels of GFP fluorescence to which aNSC transitions would correspond, we sorted three subpopulations of aNSCs: GFAP-high (GFAP-GFP$^{(high)}$PROM1$^+$ EGFR$^+$), GFAP-mid (GFAP-GFP$^{(mid)}$PROM1$^+$EGFR$^+$), and GFAP-low (GFAP-GFP$^{(low)}$PROM1$^+$EGFR$^+$) as well as NPCs (GFAP-GFP$^{(neg)}$EGFR$^+$). As predicted by the single-cell data, aNSCs sorted by FACS with higher levels of GFP fluorescence expressed markers of astrocytes and self-renewal, such as *Atp1a2* and *Ntsr2* (Figures 4B and 4C). Consistent with single-cell data, aNSCs with the lowest levels of GFP fluorescence had significantly higher expression of *Dlx2* and *Dlx1* (markers of early neurogenesis) (Figure 4D; Figure S4B) but did not yet express other later makers that were more exclusively expressed in NPCs, such as *Nrxn3* and *Dcx* (Figure 4E; Figure S4C). The populations expressed equal amounts of genes detected equally in all aNSCs subpopulations, such as *Egfr* (Figure S4D). The subdivision of the aNSC population by GFP levels generally recapitulated the gene correlation module, as shown in Figure 3J; specifically, the positive correlation between markers of astrocytes and mediators of self-renewal and anti-correlation between these genes and early mediators of neurogenesis (*Dlx1* and *Dlx2*) (Figure 4F; Figure S4I). In contrast, this sorting scheme could not distinguish the aNSC-early and aNSC-mid populations, which differed in their expression of cell cycle markers (Figures S4E–S4G), probably because these two populations express GFP at similar levels. Thus, the molecular states along the spectrum of activation and differentiation predicted by single-cell analysis can be experimentally validated.

In the Spectrum of NSC Activation and Differentiation, In Vitro-Cultured NSCs Resemble In Vivo aNSCs but Exhibit a Signature of Inflammation

Cultures of primary NSCs as neurospheres have been used to study NSCs in vitro (Conti and Cattaneo, 2010; Hitoshi et al., 2002; Ma et al., 2014), although it is debated whether these cells are good models for in vivo NSCs (Conti and Cattaneo, 2010; Parker et al., 2005). To understand how cultured NSCs compare with their in vivo counterparts, we performed single-cell RNA-seq of passage 3 neurospheres (NSs) cultured from FACS aNSCs sorted by FACS (Figure 5A). Single cells were filtered for quality in the same manner as in vivo cells (Figure S5A), resulting in 62 high-quality single-cell RNA-seq datasets. To determine where cultured NS single cells fall on the spectrum of activation and differentiation of in vivo neural progenitors, we performed PCA using the consensus-ordering genes (Table S7) on all of our in vivo single qNSCs, aNSCs, and NPCs and projected the

single NS cells onto this PCA space (Figure 5B). This analysis revealed that single NS cells most closely resemble the aNSC-mid population (proliferative aNSCs that have not yet begun to express neuronal differentiation markers) with respect to the expression of key genes that define the activation and differentiation of NSCs. However, when PCA was performed using all in vivo cells and in vitro neurosphere single cells, the neurospheres cluster separately from the in vivo lineage (Figure S5C), suggesting that there are also significant differences between the in vivo and in vitro states. Differential expression using SCDE between the cultured NS single cells and in vivo aNSCs or NPCs revealed that many of the genes significantly enriched in the in vivo populations are markers of neuronal differentiation, such as *Dlx2*, *Dcx*, *Nrxn3*, and *Dlx6as1* (Figure 5D; Figure S5B; Table S9). This is consistent with the notion that cultured neurospheres do not express markers of neuronal differentiation but express markers of astrocytes (Figure 5D Figure S5B), likely representing an undifferentiated, self-renewing state.

To identify global pathways that are different between cultured NS cells and in vivo NSCs, we performed GSEA on genes differentially expressed between the in vivo and in vitro states (Table S9). Strikingly, pathways associated with inflammation and cytokine signaling were among those upregulated in the cultured NS cells (Figure 5C). Furthermore, genes associated with inflammatory signaling, such as *Fas* and *Ifitm3*, were highly expressed in many in vitro single cells but were not consistently detected in vivo (Figure 5E; Figure S5B). Thus, although cultured NSCs resemble aNSC-mid cells on the spectrum of NSC activation and differentiation, there are important differences between cultured neurospheres and in vivo NSCs, such as the expression of markers of inflammation. Understanding these differences could help better model NSCs in vitro.

Meta-analysis of Single Cells Isolated by Different FACS Methods Using the Power of Single-Cell Transcriptomics

A single-cell characterization of NSCs in the SVZ was recently published (Llorens-Bobadilla et al., 2015), using a different dissociation method (trypsin instead of papain) and a distinct FACS strategy (Llorens-Bobadilla et al., 2015; Figure 6A). This provides a unique opportunity to address questions regarding the identity of cells isolated by different approaches. The study by Llorens-Bobadilla et al. (2015) isolated two populations by FACS from wild-type mice: GLAST$^+$PROM1$^+$ (NSCs) and GLAST$^-$PROM1$^-$ EGFR$^+$ (TAPs) (Figure 6A), whereas we isolated four populations by FACS from GFAP-GFP transgenic mice: GFAP-GFP$^+$PROM1$^-$EGFR$^-$ (niche astrocytes), GFAP-GFP$^+$PROM1$^+$ EGFR$^-$ (qNSCs), GFAP-GFP$^+$PROM1$^+$EGFR$^+$ (aNSCs), and GFAP-GFP$^-$EGFR$^+$ (NPCs/TAPs). One main difference is that Llorens-Bobadilla et al. (2015) used the surface protein GLAST to purify NSCs from wild-type mice, whereas we isolated them using GFP from GFAP-GFP transgenic mice. Another main difference is that the study by Llorens-Bobadilla et al. (2015) did not differentiate between qNSCs and aNSCs, whereas we used the marker EGFR to distinguish aNSCs from qNSCs (Figure 6A). The method of cell dissociation and marker choices for FACS have been areas of active debate in the field of NSC biology (Codega et al., 2014; Luo et al., 2015; Mich et al.,
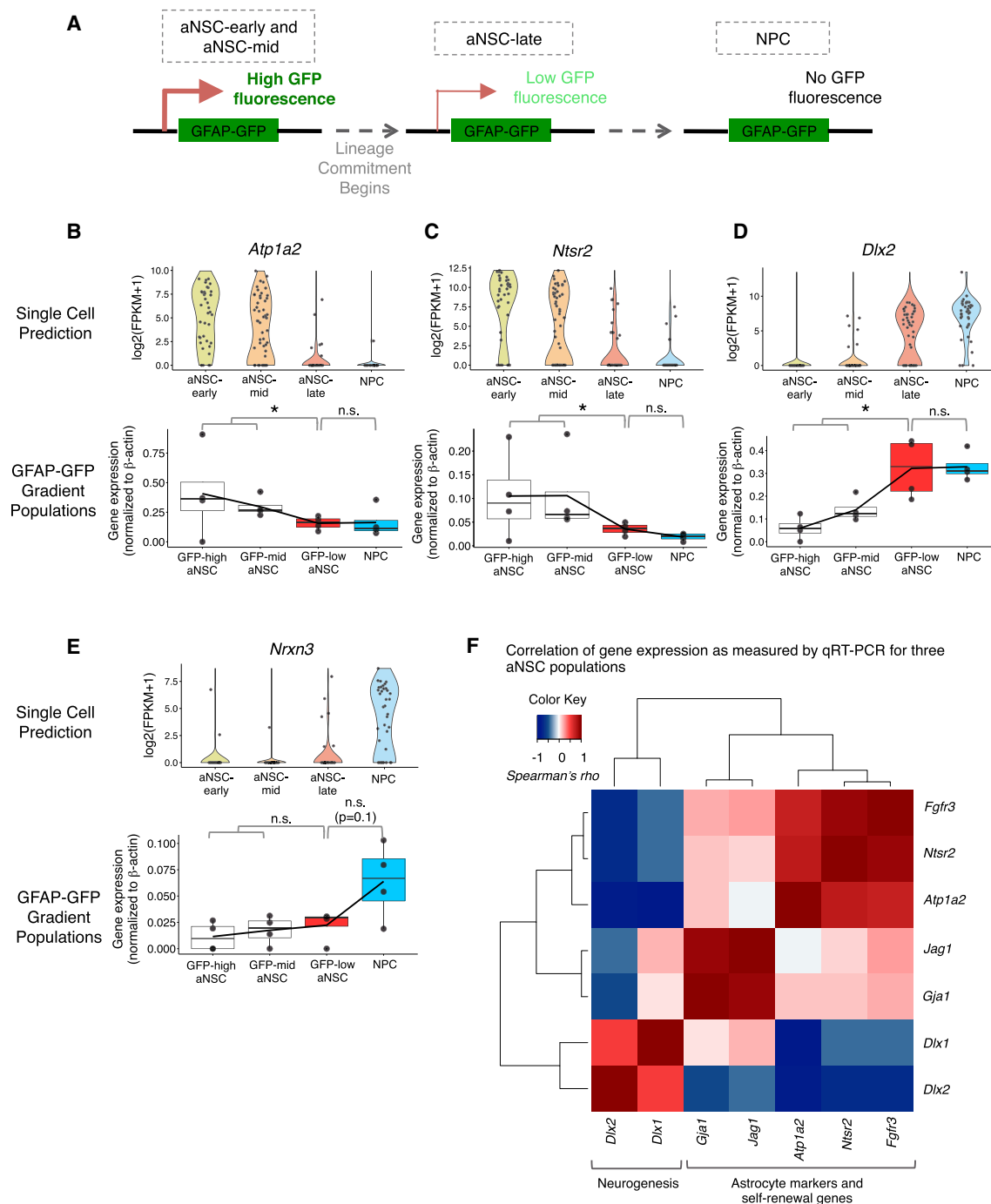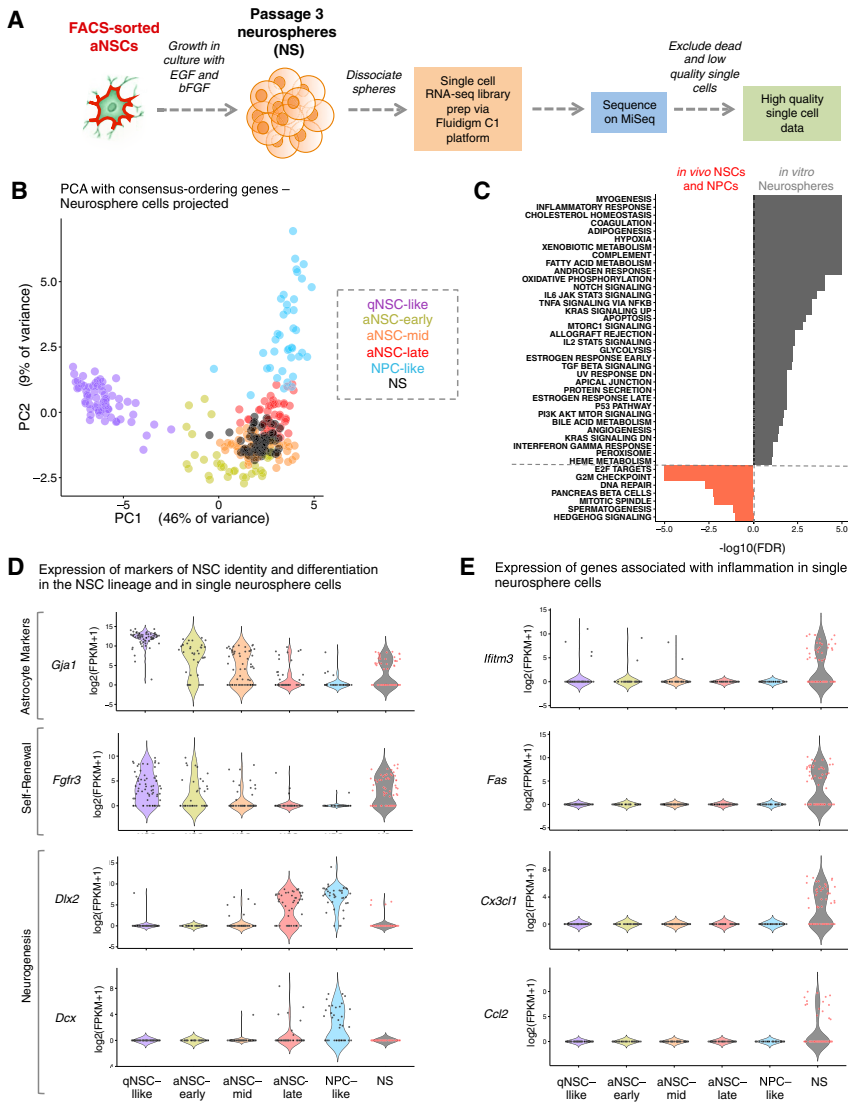
Figure 4. Experimental Validation of the Difference between aNSC-Mid and aNSCs-Late Subpopulations by Separating aNSCs Based on the Level of GFAP-GFP Expression by FACS

(A) Predicted GFP fluorescence states of aNSCs from a GFP-high state in which the GFAP-GFP promoter is active, to a GFP-low state in which the cells have committed to differentiation but retain some GFP and, finally, to the NPC state, in which cells are GFP negative.

(B–E) Top: gene expression in single cells grouped by molecular subtype as defined in Figure 3. Gene expression is expressed as log2(FPKM + 1). Bottom: gene expression was measured by qRT-PCR in subpopulations of aNSCs divided by their level of GFAP-GFP expression (GFAP-GFP-high aNSC, GFAP-GFP-mid aNSC, and GFAP-GFP-low aNSC) and NPCs. Expression shown for (B) *Atp1a2*, (C) *Ntsr2*, (D) *Dlx2*, (E) *Nrxn3*. The p values are from a one-sided Wilcoxon signed-rank test (*p ≤ 0.05).

(F) Correlation between expression of key markers of NSCs and neurogenesis in aNSC populations divided by GFAP-GFP. The carpet plot shows correlation (Spearman's rho) between individual genes in all aNSC subpopulations divided by level of GFAP-GFP. The color of the box indicates correlation (Spearman's rho) between a given gene pair (scale at top left).

A

B

PCA with consensus-ordering genes –
Neurosphere cells projected

qNSC-like
aNSC-early
aNSC-mid
aNSC-late
NPC-like
NS

C

D

Expression of markers of NSC identity and differentiation
in the NSC lineage and in single neurosphere cells

E

Expression of genes associated with inflammation in single
neurosphere cells

Figure 5. In the Spectrum of NSC Activation and Differentiation In Vivo, In Vitro-Cultured Neurospheres Resemble aNSCs but Exhibit a Signature of Inflammation

(A) Preparation of single cell RNA-seq libraries from passage 3 neurospheres (NS) derived from aNSCs sorted by FACS.

(B) PCA with qNSCs, aNSCs, and NPCs using expression [log2(FPKM + 1)] of the consensus-ordering genes from machine learning models (Table S7). NS single cells are projected onto the resulting principal component space. Cells are colored by identity as defined in Figure 2G, and NS single cells are shown in black.

(C) Gene set enrichments for genes ranked by Z score for differential expression between single NS cells and in vivo aNSCs and NPCs. Enrichments expressed as [−log10(FDR)], and directionality and color indicate the intermediate state in which the gene set is enriched (FDR < 0.2).

(D) Expression of genes associated with astrocyte identity, self-renewal, and neurogenesis in in vitro NS single cells and in vivo NSCs. The violin plots show gene expression in the cellular states defined in Figure 2G as well as in NS single cells.

(E) Expression of genes associated with inflammatory signatures in single NS cells and in vivo NSCs. Data are presented as in Figure (D).

gulation of cell cycle genes (Figures 6C and S6D). Interestingly, a subset of aNSCs from the study of Llorens-Bobadilla et al. (2015) expresses high levels of cell cycle markers (Cdk1) as well as Dlx2 transcript (Figure 6D). This state is reminiscent of the aNSC-late cells described in Figure 3. Moreover, the transition from aNSCs to NPCs (TAPs), characterized by expression of neuron-associated genes such as Dcx and Dlx6as1, is also highly conserved in both datasets (Figures 6C and 6D; Figures S6C and

2014). To compare these single-cell datasets, we independently mapped the raw sequencing data from the study by Llorens-Bobadilla et al. (2015) using our pipeline. When we conducted global PCA using all cells from both studies, the primary axis of variation was defined by the study, likely because of differences in library preparation and sequencing depth (Figure S6A). However, when we projected cells used in the study of Llorens-Bobadilla et al. (2015) onto a PCA with either the consensus-ordering genes (Table S7) or the most variable genes from our study, we observed an alignment of the cell types profiled in each study (Figure 6B; Figure S6B). Furthermore, Monocle ordering with the consensus-ordering genes on the NSCs and TAPs from Llorens-Bobadilla et al. (2015) revealed that the dynamic expression of key genes with respect to pseudotime is very similar between the two datasets (Figures 6C and 6D; Figures S6C and S6D). In both datasets, quiescent NSCs high in Id3 and Clu are ordered earliest, and activation is accompanied by an upregulation of genes important for ribosome biogenesis, followed by the upre-

S6D). Importantly, although NPCs (TAPs) express some markers usually associated with type A neuroblasts (e.g., Dcx), they also express cell cycle markers (Figure S6E and S6F), unlike neuroblasts, which do not express cell cycle markers (Figure S6E; Llorens-Bobadilla et al., 2015). Thus, the transcriptional dynamics of NSC regulators captured in these divergent FACS approaches are very similar with respect to the expression of key genes dynamically regulated along the processes of activation and differentiation.

Meta-analysis of Global Gene Expression in Different Single-Cell Studies, Including SVZ and DG

We next performed a global assessment of the similarities between NSC lineages in our study and the study of Llorens-Bobadilla et al. (2015) using all genes. We first ranked all detected genes in our dataset by their average pseudotime of expression (APE) (Figure 7A). APE represents the average pseudotime of all cells expressing a given gene for all qNSCs, aNSCs, and NPCs
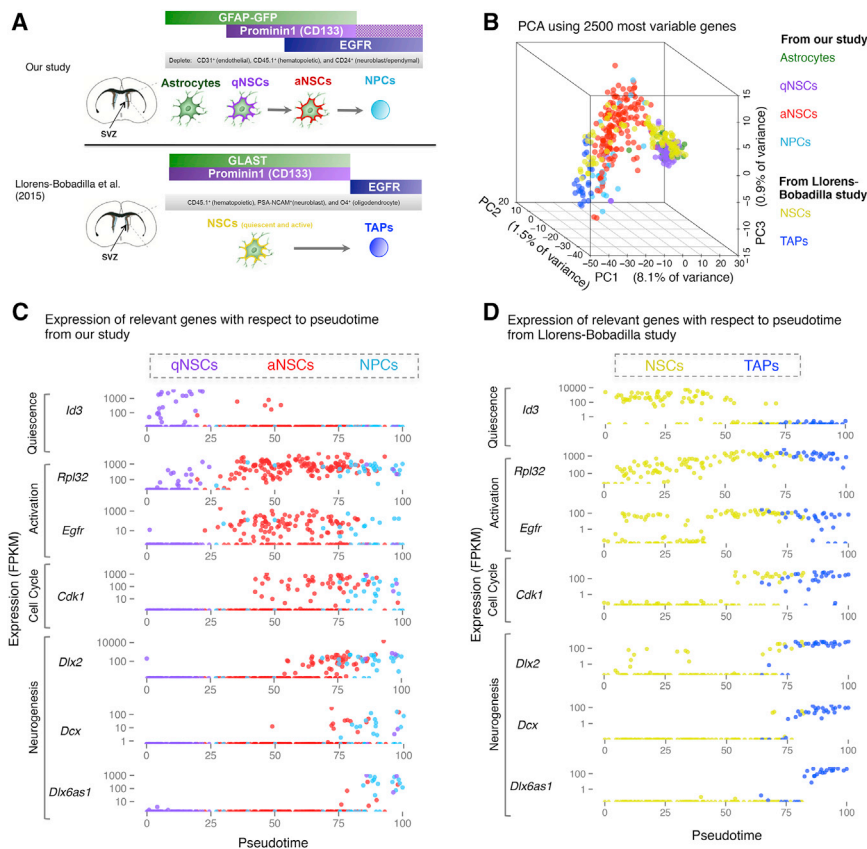
Figure 6. Meta-analysis to Compare Single Cell Identities of SVZ NSCs Isolated Using Divergent FACS Strategies

(A) Comparison of FACS schemes implemented in our study and in the study of Llorens-Bobadilla et al. (2015).

(B) PCA on all qNSCs, aNSCs, and NPCs from our study, using the expression [log2(FPKM + 1)] of the 2,500 most variable genes in these cells. All NSCs and TAPs from the study of Llorens-Bobadilla et al. (2015) are projected onto the resulting principal component space. Cells are colored by FACS-sorting identity, as indicated on the right.

(C and D) Regulators of activation and differentiation exhibit similar dynamics in NSCs and progeny isolated by divergent FACS schemes. Expression (FPKM) of key markers of activation and differentiation in each cell are plotted as a function of pseudotime generated by Monocle ordering using the consensus-ordering genes identified by machine learning (Table S7) for (C) all qNSCs, aNSCs, and NPCs from our study and (D) NSCs and TAPs analyzed by Llorens-Bobadilla et al. (2015). Cells are colored by FACS identity, as indicated on top.

sequenced at much lower depth than those from the study of Llorens-Bobadilla et al. (2015), these results also suggest that low-throughput sequencing is sufficient to capture complex transcriptional dynamics in single cells.

ordered by Monocle using the consensus-ordering genes (Table S7). Pseudotime expression heatmaps (Supplemental Experimental Procedures) for the qNSCs, aNSCs, and NPCs in our study and for the NSCs and TAPs from Llorens-Bobadilla et al. (2015) revealed that most detected genes show a high similarity in their expression profile (Figure 7B). Furthermore, the genes exclusively expressed in NPCs (or TAPs) are highly conserved between the two datasets (Figure 7C). The correlation between the APE rankings, when genes are independently ranked by APE using the two datasets, was excellent between our dataset and the dataset of Llorens-Bobadilla et al. (2015) (Figure 7D; Spearman's rho = 0.63). The agreement between the global expression profiles of these cells is striking, considering the different FACS isolation protocols and the different depths to which the cells were sequenced. The correlation between the independent APE gene rankings for the cells from our study and the differentiating myoblasts from (Trapnell et al., 2014) was still positive but much lower (Figure 7E; Spearman's rho = 0.17). Thus, the correlation between the SVZ NSC datasets cannot be solely attributed to cell cycle entry. Similar results were obtained when we performed Monocle ordering using the consensus-ordering genes with the normalized expression values provided by Llorens-Bobadilla et al. (2015) and Trapnell et al. (2014) (Figures S7B, S7C, S7F, and S7G). The concordance between our study and that of Llorens-Bobadilla et al. (2015) suggests global similarities between the lineages isolated in these two studies. Because our RNA-seq libraries were

We next extended this type of analysis to other NSC single-cell datasets. Shin and colleagues generated 142 single-cell RNA-seq datasets from hippocampal NSCs (Shin et al., 2015). The overall gene expression pattern in single NSCs from the hippocampus was similar to that of the SVZ (Figure S7D), and there was positive correlation in independent gene rankings by APE for our study and hippocampal NSCs profiled by Shin et al. (2015) (Figure 7F; Spearman's rho = 0.38). This correlation was higher than the gene ranking correlation between SVZ NSCs and differentiating myoblasts, suggesting similarities between neurogenic niches beyond general processes of cell proliferation. Similar results were observed using the consensus-ordering genes (Figures S7E and S7H). Thus, the primary gene signatures of quiescence and activation may be conserved in the neurogenic niches in the adult brain.

This meta-analysis indicates that the NSC lineages identified by divergent FACS schemes resulted in the isolation of very similar cells and suggests similarities between the gene signatures of quiescence and activation in the two different adult neurogenic niches.

DISCUSSION

Our single-cell RNA-seq on cells from four purified populations from the adult mouse SVZ—niche astrocytes, qNSCs, aNSCs, and NPCs, reveals heterogeneity and transcriptional dynamics in the adult neural stem cell lineage. Our data revealed that
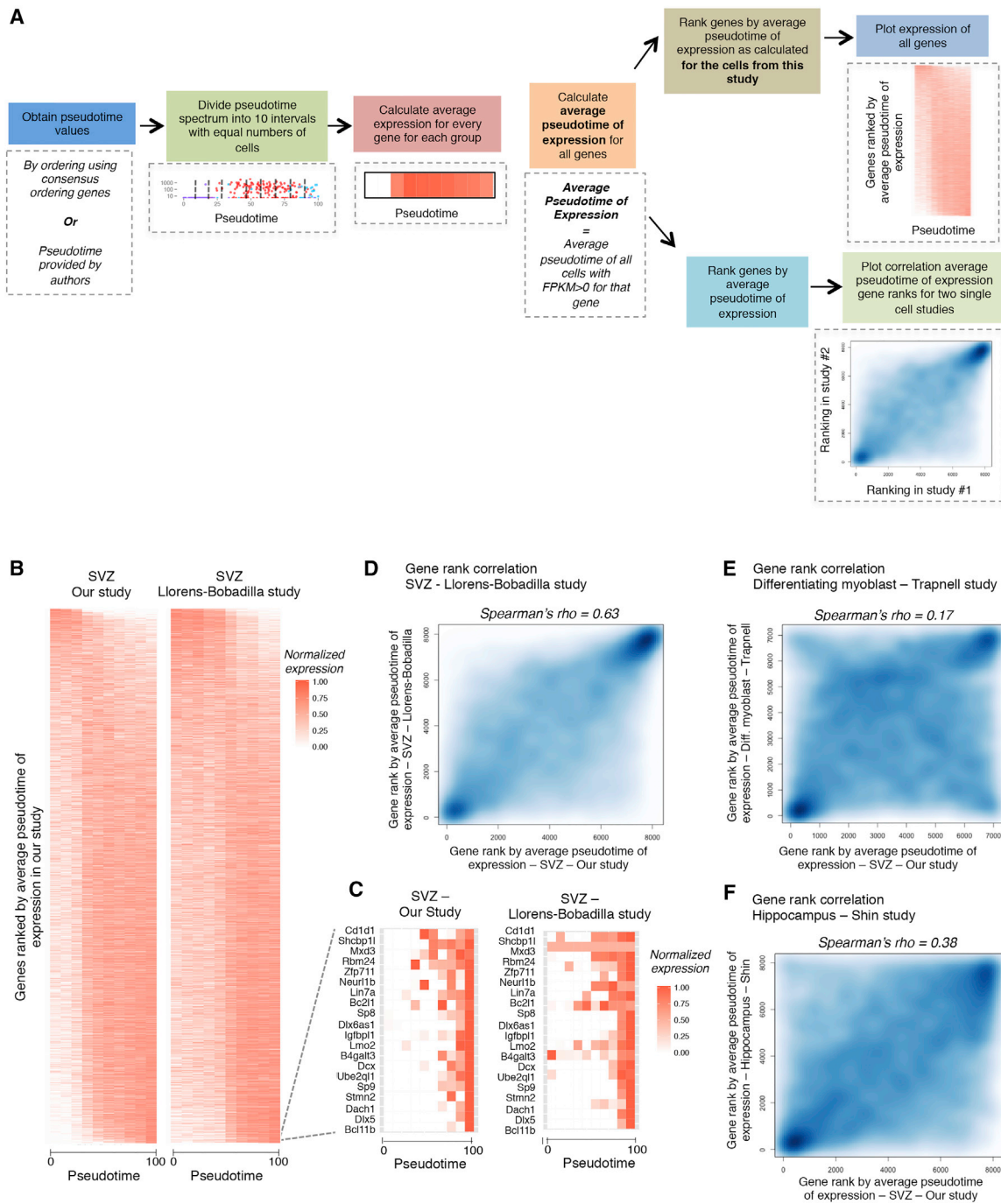
Figure 7. Meta-analysis to Compare Global Pseudotime-Dependent Gene Expression in Various Single-Cell Datasets

(A) Schematic outlining the approaches for generating pseudotime expression heatmaps and for correlating gene rankings by APE (Supplemental Experimental Procedures) for different single-cell datasets.

(B) Heatmap representing the expression of all detected genes ranked by APE defined in our study. Expression is plotted as a function of pseudotime. Left: expression from our study (qNSCs, aNSCs, and NPCs) and pseudotime defined by Monocle ordering using consensus-ordering genes identified by machine learning (Table S7). Right: expression from the study of Llorens-Bobadilla et al. (2015) (NSCs and TAPs) and pseudotime defined by Monocle ordering using consensus-ordering genes (Table S7).

(C) Heatmap representing expression of the 20 genes with the highest values of APE (expressed most exclusively in NPCs) in our dataset. Left: expression from our study (qNSCs, aNSCs, and NPCs) and pseudotime defined as in (B). Right: expression from the study of Llorens-Bobadilla et al. (2015) (NSCs and TAPs) and pseudotime defined as in (B).

(legend continued on next page)

FACS aNSCs sorted by FACS can be divided into three groups along the process of activation and differentiation: aNSC-early, aNSC-mid, and aNSC-late. The aNSC-late subpopulation can be enriched by sorting aNSCs with low levels of GFAP-GFP. In the future, excluding the population of cells expressing GFAP-GFP at low levels may allow for the enrichment of the earliest, putatively self-renewing stem cells using FACS.

The power of single-cell profiling also allowed us to perform a global comparison with other single-cell studies. The high correlation between the identities of the single cells profiled in the study of Llorens-Bobadilla et al. (2015) and our study is highly instructive for FACS protocols for in vivo NSCs. In our protocol (based on Codega et al., 2014), we used the enzyme papain to digest the SVZ for FACS, and we have found that papain cleaves GLAST (B.W.D., D.S.L., and A.B., unpublished data), the marker that was used in the study of Llorens-Bobadilla et al. (2015). Thus, an enzyme other than papain should be used when sorting by GLAST (and, indeed, Llorens-Bobadilla et al., 2015, used trypsin). Our meta-analysis of single-cell data is encouraging for the field of NSC biology because it suggests that divergent methods for isolating or identifying the SVZ NSCs that use either GFAP-GFP (Beckervordersandforth et al., 2010; Codega et al., 2014; Fischer et al., 2011) or GLAST (Calzolari et al., 2015; Llorens-Bobadilla et al., 2015; Mich et al., 2014) isolate very similar cell types from the SVZ. Furthermore, the similarities of the pseudotime-related expression profiles of quiescent and active NSCs from the hippocampus (Shin et al., 2015) and SVZ (Llorens-Bobadilla et al., 2015 and our study) suggest that the molecular phenotypes of quiescence and activation in these cell types are at least partially conserved.

As technology for sequencing hundreds and even thousands of single cells emerges (Cadwell et al., 2016; Fan et al., 2015; Habib et al., 2016; Klein et al., 2015; Macosko et al., 2015), it is likely that the single-cell characterization of the adult NSC lineage will continue to improve. These developments will complement other methods for characterizing in vivo cell heterogeneity, such as lineage tracing, to provide more complete definitions of adult stem cell lineages (Goodell et al., 2015; Merkle et al., 2014). The knowledge of transcriptional dynamics and cell fate decisions as NSCs activate and commit to differentiation should provide key targets for recruiting NSCs or directing their differentiation. The improved definition of the NSC lineage at the single-cell level should also facilitate the study of NSCs in the context of aging and disease.

EXPERIMENTAL PROCEDURES

NSC Isolation from Adult Mouse Brains
Animal procedures were conducted under APLAC protocol #8661. For single-cell RNA-seq library generation of in vivo cells, four 3-month-old male GFAP-GFP mice (the Jackson Laboratory, catalog no.003257) were euthanized, and brains were immediately harvested. As described in Codega et al. (2014, the SVZ from each hemisphere was micro-dissected. The SVZ was dissociated

with enzymatic digestion with papain for 10 min at a concentration of 14 U/mL. The dissociated SVZ was then titrated in a solution containing 0.7 mg/mL ovomucoid and 0.5 mg/mL DNaseI in DMEM/F12. The dissociated SVZ was then centrifuged through 22% Percoll in PBS to remove myelin debris. Following centrifugation through Percoll solution, cells were washed with FACS buffer (Hank's balanced salt solution [HBSS], 1% BSA, 1% glucose). Antibody staining was carried out in FACS buffer at the following dilutions: Prom1-Biotin (eBioscience, catalog no. 13-1331-80, 1:300), EGF-Alexa Fluor 647 (Life Technologies, catalog no. E35351, 1:300), CD24-PacBlue (eBioscience, catalog no. 48-0242-80, 1:400), CD31-phycoerythrin (PE) (eBioscience, catalog no. 12-0311-81, 1:50), CD45-BV605 (BioLegend, catalog no. 110737, 1:50), and Strep-PECy7 (eBioscience, catalog no. 25-4517-82, 1:500). FACS was performed on a BD FACS Aria II sorter using a 100-μm nozzle at 13.1 psi. Cell gates were defined as follows (Codega et al., 2014):

Astrocytes: (GFAP-GFP)$^+$ PROM1$^-$CD31$^-$CD24$^-$CD45$^-$
qNSCs: (GFAP-GFP)$^+$PROM1$^+$EGFR$^-$CD31$^-$CD24$^-$CD45$^-$
aNSCs: (GFAP-GFP)$^+$PROM1$^+$EGFR$^+$CD31$^-$CD24$^-$CD45$^-$
NPCs: (GFAP-GFP)$^-$EGFR$^+$CD31$^-$CD24$^-$CD45$^-$
Endothelial cells: (GFAP-GFP)$^-$CD31$^-$

Cells were sorted into catching medium: DMEM/F12 with B27 (1:50), B27 supplement (Thermo Fisher, no vitamin A, 1:50), N2 supplement (Thermo Fisher, 1:100), 15 mM (4-(2-hydroxyethyl)-1-piperazineethanesulfonic acid) (HEPES) buffer, 0.6% glucose, penicillin-streptomycin-glutamine (Life Technologies, 1:100), and insulin-transferrin-selenium (Life Technologies, 1:1000). Cells were then spun down at 300 × g at 4°C and resuspended in catching medium at a concentration of 300 cells/μL.

Single-Cell RNA-Seq Library Preparation
A 300 cells/μL cell solution was mixed at a 7:3 ratio with Fluidigm C1 suspension reagent, and this solution was loaded onto a small (5–10 μm) Fluidigm C1 Single-Cell Auto Prep chip for all in vivo single cells studied and a medium (10–17 μm) Fluidigm C1 Single-Cell Auto Prep chip for in vitro-cultured neurosphere-derived single cells. Live/dead staining was performed using Fluidigm live/dead cell staining solution as described in the Fluidigm C1 mRNA-seq protocol and imaged using a Leica DMI4000B microscope. Reverse transcription and PCR was performed directly on the chip using the SMARTer chemistry kit from Clontech, and PCR was also performed on the chip using the Advantage PCR kit (SMARTer Ultra Low RNA Kit for the Fluidigm C1, Clontech, catalog no. 634832). The resulting cDNA was transferred to a 96-well plate, and a subset of representative samples was analyzed by BioAnalyzer. A quarter of the cDNA for each library was quantified using the Quant-iT PicoGreen dsDNA assay kit (Thermo Fisher, catalog no. P11496) and verified to be within a range of 0.1–0.5 ng/μL (or diluted, when necessary, with C1 DNA dilution buffer). Sequencing libraries were prepared directly in a 96-well plate using the Nextera XT library preparation kit (Illumina, catalog no. FC-131-1024). Each library was individually barcoded using the Nextera XT 96 sample index kit (Illumina, catalog no. FC-131-1002), and all 96 barcoded libraries from each chip were pooled into single multiplexed libraries. The DNA concentration of multiplexed libraries was measured using BioAnalyzer. These multiplexed libraries were sequenced using either Illumina MiSeq (Illumina) or HiSeq2000 (Illumina) at a concentration of 2 pM. Details can be found in Table S1.

Construction of a Machine Learning Model and Determination of Consensus-Ordering Genes
We carried out a four-way classification between the following groups that correspond to key states/subpopulations: qNSCs, cell cycle low aNSCs, cell

---

(D) Smooth scatterplot representing gene ranks by APE in (x axis) qNSCs, aNSCs, and NPCs from our study ordered by Monocle using the consensus-ordering genes identified by machine learning (Table S7) and (y axis) NSCs and TAPs from the study of Llorens-Bobadilla et al. (2015) ordered by Monocle using the consensus-ordering genes identified by machine learning (Table S7) (Spearman's rho = 0.63, p < 2.2e^{-16}).

(E) Smooth scatterplot representing gene rankings by APE in (x axis) qNSCs, aNSCs, and NPCs from the current study ordered as in (D) and (y axis) differentiating myoblasts ordered by Monocle from Trapnell et al. (2014) (Spearman's rho = 0.17, p < 2.2e^{-16}).

(F) Smooth scatterplot representing gene rankings by APE in (x axis) qNSCs, aNSCs, and NPCs from our study ordered as in (D) and (y axis) hippocampal NSCs ordered by Waterfall in the study by Shin et al. (2015) (Spearman's rho = 0.38, p < 2.2e^{-16}).

cycle high aNSCs, and NPCs. Classification was carried out by implementing a stochastic gradient-boosted classification model using the Comprehensive R Archive Network (R CRAN) package generalized boosted regression models (GBM) v2.1.1. Briefly, 20 single cells from each group (training set) were randomly selected and subjected to GBM modeling as implemented by the Caret package v.6.0-58 in R. The accuracy of the model was tested on cells that were not used for the training set. The GBM classification was bootstrapped by repeatedly sampling 20 cells from each group and building an independent model. In total, 100 GBM models were built. Following construction of the models, the top 100 features from each of the 100 models were obtained. A consensus set of ordering genes was built using genes that were in the top 100 most important features of at least half of the classification models or in the top 100 most important features of at least 25% of the models (Table S7).

Ordering Cells with Monocle Using Consensus-Ordering Genes

Monocle ordering was conducted for all qNSCs, aNSCs, and NPC cells using the set of consensus-ordering genes (Table S7) identified by machine learning. The expression of genes of interest was plotted with respect to pseudotime. The resulting pseudotime expression spectrum was divided according to the expression of genes of interest. The approach used to divide the pseudotime expression spectrum is enumerated below:

qNSC-like to aNSC-early – Earliest pseudotime at which *Rpl4*, *Rpl32*, and *Egfr* are predominantly expressed
aNSC-early to aNSC-mid – Earliest pseudotime at which *Ccna2*, *Cdk1*, and *Ccnb2* are predominantly expressed
aNSC-mid to aNSC-late – Earliest pseudotime at which *Dlx1* and *Dlx2* are predominantly expressed
aNSC-late to NPC-like – Earliest pseudotime at which *Nrxn3*, *Dlx6as1*, and *Dcx* are predominantly expressed

Differential expression between the putative groups was conducted using the R package SCDE v1.2.1 (Kharchenko et al., 2014), and genes were ranked by *Z* score for differential expression between groups. Pathway enrichment was performed on ranked lists with GSEA using GO Biological Process and contains related neuroepithelial cell identity (Lein et al., 2007) lists.

ACCESSION NUMBERS

The accession number for the data reported in this paper is BioProject: PRJNA324289. Code is available at https://github.com/bdulken/SVZ_NSC_Dulken_2.

SUPPLEMENTAL INFORMATION

Supplemental Information includes Supplemental Experimental Procedures, seven figures, and nine tables and can be found with this article online at http://dx.doi.org/10.1016/j.celrep.2016.12.060.

AUTHOR CONTRIBUTIONS

B.W.D. designed and performed the experiments and analyzed the data with guidance from A.B. D.S.L. optimized the FACS of NSCs and provided the RNA-seq population datasets. S.C.B. helped with single-cell library preparation. K.H. assisted with statistical analysis and code. B.W.D. wrote the paper with the help from A.B., and all authors read the paper and provided comments.

ACKNOWLEDGMENTS

REFERENCES

Andersen, J., Urbán, N., Achimastou, A., Ito, A., Simic, M., Ullom, K., Martynoga, B., Lebel, M., Göritz, C., Frisén, J., et al. (2014). A transcriptional mechanism integrating inputs from extracellular signals to activate hippocampal stem cells. Neuron *83*, 1085–1097.

Beckervordersandforth, R., Tripathi, P., Ninkovic, J., Bayam, E., Lepier, A., Stempfhuber, B., Kirchhoff, F., Hirrlinger, J., Haslinger, A., Lie, D.C., et al. (2010). In vivo fate mapping and expression analysis reveals molecular hallmarks of prospectively isolated adult neural stem cells. Cell Stem Cell *7*, 744–758.

Bonaguidi, M.A., Peng, C.Y., McGuire, T., Falciglia, G., Gobeske, K.T., Czeisler, C., and Kessler, J.A. (2008). Noggin expands neural stem cells in the adult hippocampus. J. Neurosci. *28*, 9194–9204.

Cadwell, C.R., Palasantza, A., Jiang, X., Berens, P., Deng, Q., Yilmaz, M., Reimer, J., Shen, S., Bethge, M., Tolias, K.F., et al. (2016). Electrophysiological, transcriptomic and morphologic profiling of single neurons using Patch-seq. Nat. Biotechnol. *34*, 199–203.

Cahoy, J.D., Emery, B., Kaushal, A., Foo, L.C., Zamanian, J.L., Christopherson, K.S., Xing, Y., Lubischer, J.L., Krieg, P.A., Krupenko, S.A., et al. (2008). A transcriptome database for astrocytes, neurons, and oligodendrocytes: a new resource for understanding brain development and function. J. Neurosci. *28*, 264–278.

Calzolari, F., Michel, J., Baumgart, E.V., Theis, F., Götz, M., and Ninkovic, J. (2015). Fast clonal expansion and limited neural stem cell self-renewal in the adult subependymal zone. Nat. Neurosci. *18*, 490–492.

Codega, P., Silva-Vargas, V., Paul, A., Maldonado-Soto, A.R., Deleo, A.M., Pastrana, E., and Doetsch, F. (2014). Prospective identification and purification of quiescent adult neural stem cells from their in vivo niche. Neuron *82*, 545–559.

Conti, L., and Cattaneo, E. (2010). Neural stem cell systems: physiological players or in vitro entities? Nat. Rev. Neurosci. *11*, 176–187.

Doetsch, F., Caillé, I., Lim, D.A., García-Verdugo, J.M., and Alvarez-Buylla, A. (1999). Subventricular zone astrocytes are neural stem cells in the adult mammalian brain. Cell *97*, 703–716.

Doetsch, F., Petreanu, L., Caille, I., Garcia-Verdugo, J.M., and Alvarez-Buylla, A. (2002). EGF converts transit-amplifying neurogenic precursors in the adult brain into multipotent stem cells. Neuron *36*, 1021–1034.

Fan, H.C., Fu, G.K., and Fodor, S.P.A. (2015). Expression profiling. Combinatorial labeling of single cells for gene expression cytometry. Science *347*, 1258367.

Fischer, J., Beckervordersandforth, R., Tripathi, P., Steiner-Mezzadri, A., Ninkovic, J., and Götz, M. (2011). Prospective isolation of adult neural stem cells from the mouse subependymal zone. Nat. Protoc. *6*, 1981–1989.

Friedman, J.H. (2002). Stochastic gradient boosting. Comput. Stat. Data Anal. *38*, 367–378.

Garcia, A.D., Doan, N.B., Imura, T., Bush, T.G., and Sofroniew, M.V. (2004). GFAP-expressing progenitors are the principal source of constitutive neurogenesis in adult mouse forebrain. Nat. Neurosci. *7*, 1233–1241.

Goodell, M.A., Nguyen, H., and Shroyer, N. (2015). Somatic stem cell heterogeneity: diversity in the blood, skin and intestinal stem cell compartments. Nat. Rev. Mol. Cell Biol. *16*, 299–309.

Habib, N., Li, Y., Heidenreich, M., Swiech, L., Trombetta, J.J., Zhang, F., and Regev, A. (2016). Div-Seq: A single nucleus RNA-Seq method reveals dynamics of rare adult newborn neurons in the CNS. Science *353*, 925–928.

Haghverdi, L., Buettner, F., and Theis, F.J. (2015). Diffusion maps for high-dimensional single-cell analysis of differentiation data. Bioinformatics *31*, 2989–2998.

Hitoshi, S., Alexson, T., Tropepe, V., Donoviel, D., Elia, A.J., Nye, J.S., Conlon, R.A., Mak, T.W., Bernstein, A., and van der Kooy, D. (2002). Notch pathway molecules are essential for the maintenance, but not the generation, of mammalian neural stem cells. Genes Dev. *16*, 846–858.

Hsieh, J. (2012). Orchestrating transcriptional control of adult neurogenesis. Genes Dev. *26*, 1010–1021.

Kharchenko, P.V., Silberstein, L., and Scadden, D.T. (2014). Bayesian approach to single-cell differential expression analysis. Nat. Methods *11*, 740–742.

Klein, A.M., Mazutis, L., Akartuna, I., Tallapragada, N., Veres, A., Li, V., Peshkin, L., Weitz, D.A., and Kirschner, M.W. (2015). Droplet barcoding for single-cell transcriptomics applied to embryonic stem cells. Cell *161*, 1187–1201.

Lein, E.S., Hawrylycz, M.J., Ao, N., Ayres, M., Besinger, A., Bernard, A., Boe, A.F., Boguski, M.S., Brockway, K.S., Byrnes, E.J., et al. (2007). Genome-wide atlas of gene expression in the adult mouse brain. Nature *445*, 168–176.

Llorens-Bobadilla, E., Zhao, S., Baser, A., Saiz-Castro, G., Zwadlo, K., and Martin-Villalba, A. (2015). Single-Cell Transcriptomics Reveals a Population of Dormant Neural Stem Cells that Become Activated upon Brain Injury. Cell Stem Cell *17*, 329–340.

Long, J.E., Swan, C., Liang, W.S., Cobos, I., Potter, G.B., and Rubenstein, J.L.R. (2009). Dlx1&2 and Mash1 transcription factors control striatal patterning and differentiation through parallel and overlapping pathways. J. Comp. Neurol. *512*, 556–572.

Luo, Y., Coskun, V., Liang, A., Yu, J., Cheng, L., Ge, W., Shi, Z., Zhang, K., Li, C., Cui, Y., et al. (2015). Single-cell transcriptome analyses reveal signals to activate dormant neural stem cells. Cell *161*, 1175–1186.

Ma, C.Y., Yao, M.J., Zhai, Q.W., Jiao, J.W., Yuan, X.B., and Poo, M.M. (2014). SIRT1 suppresses self-renewal of adult hippocampal neural stem cells. Development *141*, 4697–4709.

Macosko, E.Z., Basu, A., Satija, R., Nemesh, J., Shekhar, K., Goldman, M., Tirosh, I., Bialas, A.R., Kamitaki, N., Martersteck, E.M., et al. (2015). Highly Parallel Genome-wide Expression Profiling of Individual Cells Using Nanoliter Droplets. Cell *161*, 1202–1214.

Maric, D., Fiorio Pla, A., Chang, Y.H., and Barker, J.L. (2007). Self-renewing and differentiating properties of cortical neural stem cells are selectively regulated by basic fibroblast growth factor (FGF) signaling via specific FGF receptors. J. Neurosci. *27*, 1836–1852.

Merkle, F.T., Fuentealba, L.C., Sanders, T.A., Magno, L., Kessaris, N., and Alvarez-Buylla, A. (2014). Adult neural stem cells in distinct microdomains generate previously unknown interneuron types. Nat. Neurosci. *17*, 207–214.

Mich, J.K., Signer, R.A., Nakada, D., Pineda, A., Burgess, R.J., Vue, T.Y., Johnson, J.E., and Morrison, S.J. (2014). Prospective identification of functionally distinct stem cells and neurosphere-initiating cells in adult mouse forebrain. eLife *3*, e02669.

Mira, H., Andreu, Z., Suh, H., Lie, D.C., Jessberger, S., Consiglio, A., San Emeterio, J., Hortigüela, R., Marqués-Torrejón, M.A., Nakashima, K., et al. (2010).

Signaling through BMPR-IA regulates quiescence and long-term activity of neural stem cells in the adult hippocampus. Cell Stem Cell *7*, 78–89.

Mirzadeh, Z., Merkle, F.T., Soriano-Navarro, M., Garcia-Verdugo, J.M., and Alvarez-Buylla, A. (2008). Neural stem cells confer unique pinwheel architecture to the ventricular surface in neurogenic regions of the adult brain. Cell Stem Cell *3*, 265–278.

Nyfeler, Y., Kirch, R.D., Mantei, N., Leone, D.P., Radtke, F., Suter, U., and Taylor, V. (2005). Jagged1 signals in the postnatal subventricular zone are required for neural stem cell self-renewal. EMBO J. *24*, 3504–3515.

Parker, M.A., Anderson, J.K., Corliss, D.A., Abraria, V.E., Sidman, R.L., Park, K.I., Teng, Y.D., Cotanche, D.A., and Snyder, E.Y. (2005). Expression profile of an operationally-defined neural stem cell clone. Exp. Neurol. *194*, 320–332.

Pastrana, E., Cheng, L.C., and Doetsch, F. (2009). Simultaneous prospective purification of adult subventricular zone neural stem cells and their progeny. Proc. Natl. Acad. Sci. USA *106*, 6387–6392.

Petryniak, M.A., Potter, G.B., Rowitch, D.H., and Rubenstein, J.L.R. (2007). Dlx1 and Dlx2 control neuronal versus oligodendroglial cell fate acquisition in the developing forebrain. Neuron *55*, 417–433.

Pollen, A.A., Nowakowski, T.J., Shuga, J., Wang, X., Leyrat, A.A., Lui, J.H., Li, N., Szpankowski, L., Fowler, B., Chen, P., et al. (2014). Low-coverage single-cell mRNA sequencing reveals cellular heterogeneity and activated signaling pathways in developing cerebral cortex. Nat. Biotechnol. *32*, 1053–1058.

Shin, J., Berg, D.A., Zhu, Y., Shin, J.Y., Song, J., Bonaguidi, M.A., Enikolopov, G., Nauen, D.W., Christian, K.M., Ming, G.L., and Song, H. (2015). Single-Cell RNA-Seq with Waterfall Reveals Molecular Cascades underlying Adult Neurogenesis. Cell Stem Cell *17*, 360–372.

Suh, Y., Obernier, K., Hölzl-Wenig, G., Mandl, C., Herrmann, A., Wörner, K., Eckstein, V., and Ciccolini, F. (2009). Interaction between DLX2 and EGFR regulates proliferation and neurogenesis of SVZ precursors. Mol. Cell. Neurosci. *42*, 308–314.

Trapnell, C., Cacchiarelli, D., Grimsby, J., Pokharel, P., Li, S., Morse, M., Lennon, N.J., Livak, K.J., Mikkelsen, T.S., and Rinn, J.L. (2014). The dynamics and regulators of cell fate decisions are revealed by pseudotemporal ordering of single cells. Nat. Biotechnol. *32*, 381–386.

Waclaw, R.R., Allen, Z.J., 2nd, Bell, S.M., Erdélyi, F., Szabó, G., Potter, S.S., and Campbell, K. (2006). The zinc finger transcription factor Sp8 regulates the generation and diversity of olfactory bulb interneurons. Neuron *49*, 503–516.

Wu, A.R., Neff, N.F., Kalisky, T., Dalerba, P., Treutlein, B., Rothenberg, M.E., Mburu, F.M., Mantalas, G.L., Sim, S., Clarke, M.F., and Quake, S.R. (2014). Quantitative assessment of single-cell RNA-sequencing methods. Nat. Methods *11*, 41–46.

Zhao, C., Deng, W., and Gage, F.H. (2008). Mechanisms and functional implications of adult neurogenesis. Cell *132*, 645–660.

Zhuo, L., Sun, B., Zhang, C.L., Fine, A., Chiu, S.Y., and Messing, A. (1997). Live astrocytes visualized by green fluorescent protein in transgenic mice. Dev. Biol. *187*, 36–42.